Spin-singlet order in a pyrochlore antiferromagnet

Hirokazu Tsunetsugu
Institute of Materials Science, University of Tsukuba, Tsukuba 305-8573, Japan
(Received 21 August 2001; published 14 December 2001)

The ground state of an $S=\frac{1}{2}$ quantum antiferromagnet on a pyrochlore lattice is investigated based on an effective low-energy Hamiltonian in the spin-singlet sector. In the level of the mean-field approximation, it is known that a majority part of the spins shows a long-range order of spin-singlet dimers, with a coexisting nonordered part in the singlet sector. In this paper, I first discuss elementary excitations in the ordered part and their coupling to the remaining nonordered part. Next, I derive a coupling-mediated effective interaction in the nonordered part, and examine the possibility of symmetry breaking. I find that the remaining part turns out to show a $\mathbf{q}=\mathbf{0}$ order of either dimers or tetramers. I also find that this symmetry breaking leads to low-energy singlet excitations with linear dispersions, within the harmonic approximation for quantum fluctuations. The system has a hierarchical structure of relevant energy scales, and this may be a general feature of geometrically frustrated magnets.

DOI: 10.1103/PhysRevB.65.024415 PACS number(s): 75.10.Jm, 75.40.Gb, 75.50.Ee

I. INTRODUCTION

A variety of antiferromagnets have a geometrically frustrated lattice structure, and many of them show interesting physical properties.[1] The geometrical frustration often leads to a drastic reduction of the energy scale, and a large number of spin states become degenerate or nearly degenerate in the low-energy sector as a consequence. Many experimentally observed unusual properties are ascribed to this degeneracy.

Theoretical studies have actually demonstrated the presence of a thermodynamic degeneracy of the ground state in many classical models with geometrical frustration.[2] However, this implies that we have to examine the effects of various neglected processes in the low-energy sector, in order to obtain a more complete description at low temperatures. A physical ground state should not be thermodynamically degenerate, as the third law of thermodynamics implies. The real low-temperature asymptotic behavior is determined by these additional processes, and eventually the system undergoes some kind of symmetry breaking and releases the residual entropy. The processes to consider are, for example, small spin anisotropy, longer-range spin exchanges, spin-orbit coupling, and multispin exchanges.

In this paper, I will examine the effects of another type of important process, quantum fluctuations. The classical degeneracy due to geometrical frustration is to be lifted by hybridization driven by quantum fluctuations, resulting in a nondegenerate (in the thermodynamic sense) ground state, possibly with symmetry breaking. This mechanism of long-range order may be considered as a quantum version of order by disorder, which was first proposed by Villain.[3] If the interactions are short ranged, this effect is efficient in geometrically frustrated systems, compared to randomly frustrated systems such as a spin glass. This is because degenerate states in geometrically frustrated magnets differ in their local-spin configurations, whereas the difference in spin glasses is in longer-range configurations. Therefore, quantum transition probability between different states is correspondingly larger in geometrically frustrated systems.

To examine the above scenario, in the present work I will study a Heisenberg antiferromagnet on a pyrochlore lattice, a typical example of geometrically frustrated magnets in three dimensions. The pyrochlore lattice is a network of corner-sharing tetrahedra. It is realized as a sublattice in spinel compounds and pyrochlore compounds, and there are many magnetic materials with magnetic ions on a pyrochlore lattice.[1] Since quantum fluctuations are concerned, I concentrate on the limit of large quantum fluctuations, which corresponds to the smallest spin quantum number, $S=\frac{1}{2}$.

Classical antiferromagnets on a pyrochlore lattice were studied by several groups.[2,4] They show a thermodynamically degenerate ground state for an Ising model and a classical Heisenberg model. For example, Liebmann's estimate of the ground-state entropy[2] is about $(0.293-0.296)\times\log 2$, between one-fourth and one-third of the total entropy. The classical Heisenberg model also has thermodynamically degenerate ground states. It is also believed that no phase transition takes place at finite temperatures, indicating the absence of an order-by-disorder mechanism.[3]

Recently, theoretical studies were begun for quantum antiferromagnets on a pyrochlore lattice.[5–9] The results indicate a spin-liquid nature, i.e., a spin-singlet ground state and a finite energy gap for triplet excitations. However, this spin-liquid phase is different from the one in nonfrustrated quantum antiferromagnets like spin ladders.[10] There may exist a thermodynamic number of singlet states within a spin gap in the frustrated case, while the lowest excitation is usually a spin triplet in the nonfrustrated case. Therefore, the system has a potential of revealing nontrivial symmetry breaking inside the spin-singlet sector once residual interactions between these singlet states take effect. Along this line, a low-energy effective Hamiltonian was derived, and a partial dimer order was predicted within the mean-field approximation.[5,9] Interestingly, this effective model is also frustrated, and the dimer order is only partial, and a quarter of low-energy singlet degrees of freedom remain nonordered. In this paper, I start from the same effective Hamiltonian, and will complete the above approach. I will show the presence of second-stage symmetry breaking, and determine the ultimate ground state by taking account of effects of quan-

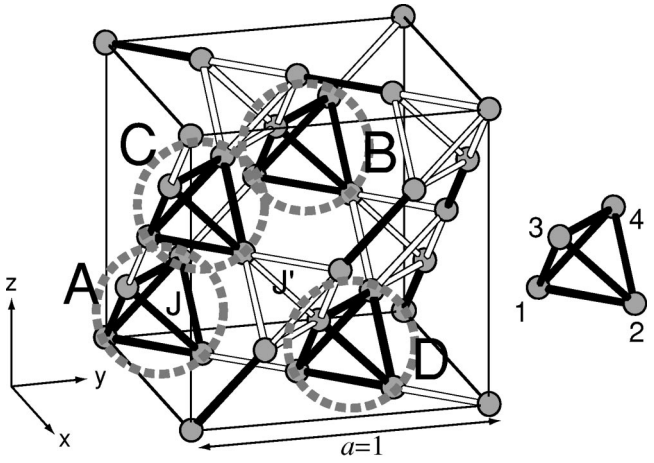

FIG. 1. Cubic unit cell of the pyrochlore lattice, containing four tetrahedra labeled $A-D$. Sites in the tetrahedron unit are labeled by indexes 1–4. Exchange couplings in the $A-D$ tetrahedra are J shown by black bonds, while intertetrahedron couplings are J' shown by white bonds.

tum fluctuations. I will also study various types of excitations.

This paper is organized as follows. In Secs. II and III, I will briefly explain the low-energy effective Hamiltonian and its mean-field ground state with partial dimer order. I will investigate elementary excitations in the ordered part, and their coupling to the nonordered part in Secs. IV and V. I will then derive the effective interaction for the nonordered part, and finally determine the long-range order of the whole system in Secs. VI and VII. Section VIII is devoted to conclusions and discussions.

II. MODEL

The model to study is the spin-$\frac{1}{2}$ Heisenberg antiferromagnet on the pyrochlore lattice:

$$H_S=\sum_{\langle \mathbf{r},\mathbf{r}'\rangle} J_{\mathbf{r},\mathbf{r}'}\mathbf{S}_r\cdot\mathbf{S}_{r'} \quad (J_{\mathbf{r},\mathbf{r}'}\geqslant 0), \tag{1}$$

where the summation is taken over nearest neighbor pairs. The structure of the pyrochlore lattice is shown in Fig. 1. Instead of studying this Hamiltonian directly, we take an alternative approach and start from a low-energy effective Hamiltonian, which will be shown in Eq. (4). The effective Hamiltonian in the spin-singlet sector was derived in Refs. 5 and 9. The basic strategy is to breakup the whole pyrochlore lattice into a set of tetrahedra shown by black bonds in Fig. 1, and to apply a perturbative approach in the ratio of the two types of coupling constants J'/J, with the hope that the uniform case $J'/J=1$ in question is qualitatively described by this approach. A similar approach was also applied to another typical geometrically frustrated model, Kagomé antiferromagnet.[11] In this section, I explain some details of the derivation which will be used in the following sections.

Let us understand the pyrochlore lattice as the fcc lattice consisting of tetrahedra (indicated by the dotted circle in Fig. 1), and label the four sublattices $A-D$. Each tetrahedron is composed of four symmetrically connected spins, having a T_d point group symmetry,[12] and the comprising spins are denoted by indexes 1–4, as shown in the figure. The lattice constant of the cubic unit cell is set to 1, and I will use it as units of length throughout this paper.

In the case of spin $\frac{1}{2}$, each tetrahedron unit has $2^4=16$ basis functions. Its total spin is $S_{\rm unit}=0$, 1, or 2, and in the limit of $J'/J=0$ it becomes a good quantum number. Even for homogeneous coupling ($J'/J=1$), spin correlation is very short ranged due to strong geometrical frustrations, indicating that low-energy dynamics may well be described in terms of only $S_{\rm unit}=0$ bases. Two of the 16 basis functions have $S_{\rm unit}=0$, and they are transformed as a basis of the E representation of the T_d group.

Instead of real bases, I use the complex chiral basis states

$$|+\rangle=\frac{1}{\sqrt{6}}(1+\hat{P}_S)[(\downarrow\downarrow\uparrow\uparrow)+e^{i\phi}(\downarrow\uparrow\downarrow\uparrow)+e^{-i\phi}(\downarrow\uparrow\uparrow\downarrow)],$$

$$|-\rangle=(|+\rangle)^* \quad (\phi=2\pi/3) \tag{2}$$

where $\hat{P}_S\equiv\Pi_j(S_j^+ + S_j^-)$ is the spin inversion operator, and up and down arrows denote the spin direction at sites 1–4 from left to right. The symbol ϕ is reserved for this special angle throughout this paper. These basis states are actually eigenfunctions of the chirality operator $\mathbf{S}_2\cdot(\mathbf{S}_3\times\mathbf{S}_4)$ defined with respect to site 1 (also with respect to the other three sites), and $|+\rangle$ and $|-\rangle$ have opposite chiralities from each other. I will make a further discussion of the chirality in Sec. III. It is also important to note that because of the complex coefficients in Eq. (2), they are not invariant with respect to the time-reversal operation. In this way, low-energy singlet degrees of freedom can be represented by these chiral states in each tetrahedron unit. The total entropy of this subspace is a quarter of the original value.

To describe the dynamics of the chirality, I introduce a pseudospin operator $\boldsymbol{\tau}=(\tau_1,\tau_2,\tau_3)$, with (pseudo)spin $S_\tau=\frac{1}{2}$, such that its third element is diagonal with respect to the chiral basis,

$$\tau_3|\pm\rangle=(\pm 1)|\pm\rangle, \quad [\tfrac{1}{2}\tau_\mu,\tfrac{1}{2}\tau_{\mu'}]=\epsilon_{\mu\mu'\mu''}\tfrac{1}{2}\tau_{\mu''}, \tag{3}$$

where μ, μ', $\mu''\in\{1,2,3\}$, and ϵ is the completely antisymmetric tensor.

Starting from the original Heisenberg model [Eq. (1)], the low-energy effective Hamiltonian was derived by means of third-order perturbation in J'/J,[9]

$$H_\tau=-\beta_1\sum_{\langle \mathbf{R},\mathbf{R}',\mathbf{R}''\rangle}[\tfrac{1}{2}-\mathbf{e}(\alpha_1)\cdot\boldsymbol{\tau}_{\mathbf{R}}][\tfrac{1}{2}-\mathbf{e}(\alpha_2)\cdot\boldsymbol{\tau}_{\mathbf{R}'}]$$
$$\times[\tfrac{1}{2}-\mathbf{e}(\alpha_3)\cdot\boldsymbol{\tau}_{\mathbf{R}''}], \tag{4}$$

where $\beta_1=\frac{1}{48}J'^3/J^2$, $\mathbf{e}(\alpha)=(\cos\alpha,\sin\alpha,0)$, and $\boldsymbol{\tau}_{\mathbf{R}}$ denotes the chirality pseudospin of the tetrahedron unit positioned at $\mathbf{R}$. The summation is taken over sets of three tetrahedron units which are nearest neighbor to each other, but not over all the possible combinations in the effective fcc

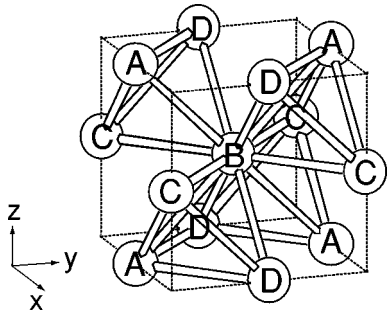

FIG. 2. Pseudospin network in the pyrochlore lattice. Pseudospins are shown by balls with sublattices labeled $A-D$. Interactions in Eq. (4) are defined for all triangular faces on each tetrahedron shown in this figure.

lattice of tetrahedra. It should be taken over a half of them, as shown in Fig. 2. In other words, the lattice of tetrahedra is equivalent to the fcc lattice concerning the ''site position,'' but the connectivity is different. Despite this difference, I will call it a fcc lattice in this paper. The details of the derivation of the effective model [Eq. (4)] are explained in Ref. 9.

The complication of model (4) lies in the nonlocality of the α parameters. The parameter α_1 for the pseudospin at position $\mathbf{R}$ depends on the sublattice label of $\mathbf{R}$, but it is not uniquely determined. It also depends on the sublattice index of the other two positions $\mathbf{R}'$ and $\mathbf{R}''$, and this is also the case for α_2 and α_3. The values of these parameters are listed in Table I.

III. MEAN-FIELD ORDER OF PSEUDOSPINS

The mean-field ground state of the effective Hamiltonian [Eq. (4)] was obtained in Ref. 9. It is done by treating the chirality pseudospins $\boldsymbol{\tau}$'s as classical unit vectors, and the configurations with the lowest energy were found. One of the four solutions is

$$\langle \boldsymbol{\tau}_{\mathbf{R}} \rangle = (\cos\theta_{\mathbf{R}}, \sin\theta_{\mathbf{R}}, 0), \quad \theta_{\mathbf{R}} = \begin{cases} \pi+\phi & (A \text{ sublattice}) \\ \text{free} & (B \text{ sublattice}) \\ \pi & (C \text{ sublattice}) \\ \pi-\phi & (D \text{ sublattice}), \end{cases} \tag{5}$$

and the other three solutions are obtained from this one by using symmetry operation of the effective Hamiltonian. I will use solutions (5) in this paper, but the other solutions are also equivalent except for a different sublattice position of free pseudospins. These solutions agree with the result of Ref. 5.

TABLE I. α parameters in Hamiltonian (4), dependent on the combination of sublattice index of three sites, $\langle \mathbf{R}\mathbf{R}'\mathbf{R}'' \rangle$.

Sublattice combination	α (A)	α (B)	α (C)	α (D)
BCD	-	ϕ	$-\phi$	0
ACD	ϕ	-	0	$-\phi$
ABD	$-\phi$	0	-	ϕ
ABC	0	$-\phi$	ϕ	-

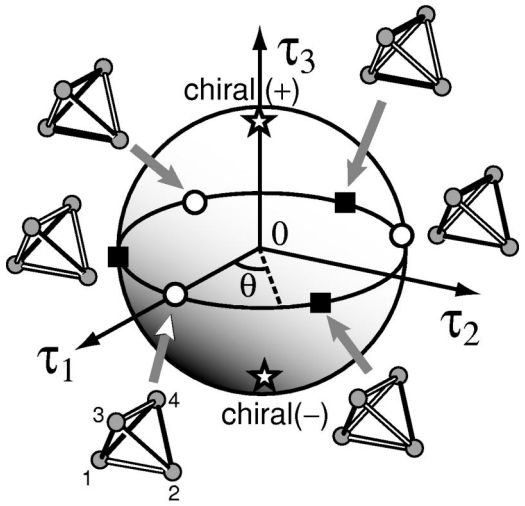

FIG. 3. Pseudospin order and spin states in tetrahedron. North and south poles correspond to a pure chiral state, and on the equator the spin states have no time-reversal symmetry breaking. Three special points with azimuthal angle $\theta=\pi$ and $\pi\pm\phi$ correspond to dimer-pair states, while the other three ($\theta=0$ and $\pm\phi$) correspond to tetramer states. Dimers and tetramers are shown in black.

The symmetry of the effective Hamiltonian in chirality space is planarlike, and interactions do not exist in the τ_3 direction. There also exists an in-plane anisotropy as described by the $\mathbf{e}(\alpha)$ vector. Therefore, this mean-field ground state is quite stable, and quantum fluctuations around it have small amplitudes in the ordered sublattices.

However, at the mean-field level, the chirality pseudospins in the B sublattice are completely free, and there is no effective potential which constrains the fluctuations of B-sublattice pseudospins. Therefore, in order to investigate a possible symmetry breaking in the remaining B sublattice, we need to consider small quantum fluctuations in the ordered part, and investigate their effects on the dynamics of the singlet fluctuations in the B sublattice. This is the subject of the following sections.

Here I present further discussions on the singlet fluctuations. In Sec. II, I introduced the pseudospin operator $\boldsymbol{\tau}$ to describe the internal degrees of freedom of local singlet configuration, and showed that its τ_3 component corresponds to spin chirality, i.e., the noncollinearity of the spin correlation or alternatively the finite spin current. The transverse components τ_1 and τ_2 also have a simple meaning. To see this point, let us consider a pseudospin coherent state $|\mathbf{m}\rangle$ defined by $(\boldsymbol{\tau}\cdot\mathbf{m})|\mathbf{m}\rangle=(+1)|\mathbf{m}\rangle$, where $\mathbf{m}$ is a classical unit vector. For $\mathbf{m}=(0,0,\pm1)$, the coherent state is the chiral state in Eq. (2). For $\mathbf{m}=(\cos\theta,\sin\theta,0)$, the coherent state is written as $|\theta\rangle=(|+\rangle+e^{i\theta}|-\rangle)/\sqrt{2}$. By writing this state in terms of the original spin representation, we note that there are six special points, as shown in Fig. 3. Three points, $\theta=\pi$ and $\pi\pm\phi$, represent a pair of spin-singlet dimers, while the other three,

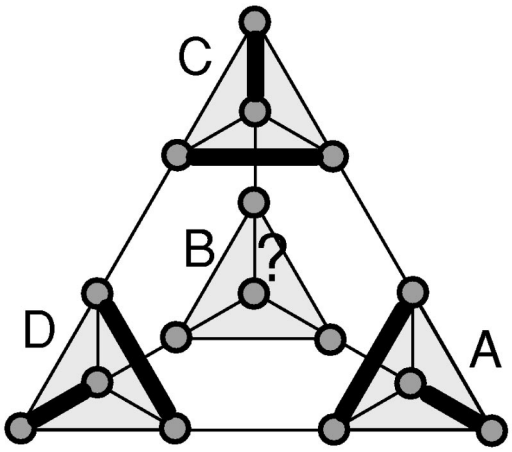

FIG. 4. A pictorial representation of the mean-field ground state [Eq. (5)]. The dimer configuration in the cubic unit cell is projected on the (111) plane. Dimers are indicated by thick black bonds. A–D label the tetrahedra shown in Fig. 1. Molecular fields are canceled on the B tetrahedron.

$\theta=0$ and $\pm\phi$, represent a spin-singlet tetramer state. For example, $|\theta=0\rangle$ is the same as the singlet ground state on a square of sites 1–4: the total singlet state is made of two spin triplets, one out of spins 1 and 2 and the other out of spins 3 and 4. We can also prove that $|\theta=0\rangle$ is real for any θ aside from the global phase factor, meaning time reversal invariant, which is consistent with a zero chirality: $\langle\theta|\tau_3|\theta\rangle=0$. Therefore, the transverse components of the pseudospin operator describe the dimer-tetramer correlations, and more generally the inhomogeneity of two-spin correlations among six bonds in the tetrahedron unit. Since the nearest-neighbor two-spin correlations are local energy, as defined in Eq. (1), the transverse components also represent energy-density fluctuations in the tetrahedron unit.

The mean-field ground state with the order parameter [Eq. (5)] means the Bose condensation of these different coherent states on the different sublattices. Therefore, the A, C, and D sublattices show the long-range order of spin-singlet dimers, and different θ values correspond to different dimer configurations among these sublattices. The dimer configuration in the cubic unit cell is shown in Fig. 4.

IV. SINGLET EXCITATIONS IN THE ORDERED PART—DIMERON

The main part of this paper starts from this section. First, I discuss the elementary excitations in the ordered sublattices A, C, and D. To this end, I bosonize pseudospin operators and employ the harmonic approximation for fluctuations. Elementary excitations obtained in this way describe spin-singlet fluctuations around the mean-field ground state, and correspond to a small-amplitude deformation of dimer configuration in space.

As for bosonization, I rewrite the effective Hamiltonian [Eq. (4)] in terms of the Holstein-Primakoff bosons.[13] This procedure is not completely trivial, since the effective Hamiltonian contains second-order terms and third-order terms of τ operators. [The first-order terms vanish identically after taking summation in Eq. (4).] Since both terms are expected to be equally important for the ground state, I decide to set the "same order" in S_τ to all the terms in Eq. (4). This is done by replacing $1/2-\mathbf{e}\cdot\boldsymbol{\tau}$ by $S_\tau-\mathbf{e}\cdot\boldsymbol{\tau}$, which returns to its original when approaching the physical value $S_\tau=1/2$. Next I locally rotate the coordination frame of τ operator in the τ_1-τ_2 plane such that the ordered moment is along the τ_1 direction in the new frame:

$$\mathbf{e}(\alpha)\cdot\boldsymbol{\tau}_{\mathbf{R}}=\mathbf{e}(\tilde{\alpha})\cdot\tilde{\boldsymbol{\tau}}_{\mathbf{R}},\quad \langle\tilde{\boldsymbol{\tau}}_{\mathbf{R}}\rangle=(1,0,0), \tag{6}$$

$$\begin{bmatrix}\tilde{\tau}_{1,\mathbf{R}}\\ \tilde{\tau}_{2,\mathbf{R}}\end{bmatrix}=U(\theta_{\mathbf{R}})^{-1}\begin{bmatrix}\tau_{1,\mathbf{R}}\\ \tau_{2,\mathbf{R}}\end{bmatrix},\quad \tilde{\tau}_{3,\mathbf{R}}=\tau_{3,\mathbf{R}}, \tag{7}$$

with

$$U(\theta)\equiv\begin{bmatrix}\cos\theta & -\sin\theta\\ \sin\theta & \cos\theta\end{bmatrix}, \tag{8}$$

$$\tilde{\alpha}=\alpha-\theta_{\mathbf{R}},\quad \theta_{\mathbf{R}}=\tan^{-1}\frac{\langle\tau_{2\mathbf{R}}\rangle}{\langle\tau_{1\mathbf{R}}\rangle}. \tag{9}$$

The next step is the Holstein-Primakoff transformation, which represents the pseudospins in terms of boson operators $b_{\mathbf{R}}$ and $b_{\mathbf{R}}^\dagger$:

$$\tilde{\tau}_{1\mathbf{R}}=2(S_\tau-b_{\mathbf{R}}^\dagger b_{\mathbf{R}}),\quad \tilde{\tau}_{2\mathbf{R}}\sim\sqrt{2S_\tau}(b_{\mathbf{R}}^\dagger+b_{\mathbf{R}}). \tag{10}$$

Here terms of order $S_\tau^{-1/2}$ or lower are neglected. Therefore, each term in Eq. (4) is represented as

$$\begin{aligned}\tfrac{1}{2}-\mathbf{e}(\alpha)\cdot\boldsymbol{\tau}_{\mathbf{R}}\rightarrow&(1-2\cos\tilde{\alpha})S_\tau-\sqrt{2S_\tau}\sin\tilde{\alpha}\,(b_{\mathbf{R}}^\dagger+b_{\mathbf{R}})\\&-2\cos\tilde{\alpha}\,b_{\mathbf{R}}^\dagger b_{\mathbf{R}},\end{aligned} \tag{11}$$

where $\tilde{\alpha}=\alpha-\tan^{-1}(\langle\tau_{2\mathbf{R}}\rangle/\langle\tau_{1\mathbf{R}}\rangle)$.

Now consider one tetrahedron consisting of A, B, C, and D sublattice units. It has four triangular faces ($\langle\mathbf{R},\mathbf{R}',\mathbf{R}''\rangle$), and the corresponding sum of the interactions [Eq. (4)] consists of two terms. One is the term which does not couple to free pseudospin at B sublattice position H_0, and the other with coupling, H_1:

$$H(ABCD)=H_0(ABCD)+H_1(ABCD), \tag{12}$$

$$\begin{aligned}&H_0(ABCD)/\beta_1\\&=-S_\tau\{[-t(b_A^\dagger+b_A)+b_A^\dagger b_A][t(b_C^\dagger+b_C)+b_C^\dagger b_C]\\&\quad+(A,C\rightarrow C,D)+(A,C\rightarrow D,A)\}\\&\quad-(3S_\tau-b_A^\dagger b_A)(3S_\tau-b_C^\dagger b_C)(3S_\tau-b_D^\dagger b_D),\end{aligned} \tag{13}$$

$$\begin{aligned}&H_1(ABCD)/\beta_1\\&=[-t(b_A^\dagger+b_A)+b_A^\dagger b_A][t(b_C^\dagger+b_C)+b_C^\dagger b_C]\mathbf{e}(2\phi)\cdot\boldsymbol{\tau}_B\\&\quad+(A,C\rightarrow C,D)\mathbf{e}(\phi)\cdot\boldsymbol{\tau}_B+(A,C\rightarrow D,A)\mathbf{e}(0)\cdot\boldsymbol{\tau}_B,\end{aligned} \tag{14}$$

where $t=\sqrt{3S_\tau/2}$.

We sum up the $H_0(ABCD)$ term for all the positions. Since we distinguish chirality pseudospins on different sublattices, it is convenient to use the cubic unit cell shown in Fig. 2 (equivalent to Fig. 1) and write the position $\mathbf{R}$ as the sum of a cubic lattice vector, $\mathbf{n}=(n_x,n_y,n_z)$, (n_x, n_y, n_z: integer), and the internal position $\boldsymbol{\delta}_\alpha$, with $\alpha\in\{A,B,C,D\}$ being the sublattice label: $\boldsymbol{\delta}_A=(0,0,0)$, $\delta_B=(0,1/2,1/2)$, $\boldsymbol{\delta}_C=(1/2,0,1/2)$, and $\boldsymbol{\delta}_D=(1/2,1/2,0)$. We also use the symbol $b_\alpha(\mathbf{n})=b_{n+\delta_\alpha}$. We further employ the harmonic approximation by neglecting the third- and fourth-terms in b and $b^\dagger$, and obtain the following Hamiltonian for the low-energy dynamics of excitations:

$$
\begin{aligned}
H_{0,HA}/\beta_1 = &-108S_\tau^3\Omega_{\mathbf{n}}+72S_\tau^2\sum_{\mathbf{n}}\sum_{\alpha=A,C,D} b_\alpha^\dagger(\mathbf{n})b_\alpha(\mathbf{n}) \\
&+\frac{3}{2}S_\tau^2\sum_{\mathbf{n}}\sum_{m,m'=0,1}[d_A(\mathbf{n}+m\mathbf{a}_z)d_C(\mathbf{n}-m'\mathbf{a}_x) \\
&+d_C(\mathbf{n}+m\mathbf{a}_y)d_D(\mathbf{n}+m'\mathbf{a}_z) \\
&+d_D(\mathbf{n}-m\mathbf{a}_x)d_A(\mathbf{n}+m'\mathbf{a}_y)], \qquad (15)
\end{aligned}
$$

where $\mathbf{a}_x$, $\mathbf{a}_y$, and $\mathbf{a}_z$ are unit vectors along the x, y, and z directions, respectively, Ω_n is the number of cubic unit cells, and $d_\alpha\equiv b_\alpha+b_\alpha^\dagger$. The first term on the right-hand side agrees with the corresponding part of the mean-field ground-state energy, $-\frac{27}{2}\beta_1\Omega_{\mathbf{n}}$, when setting $S_\tau=\frac{1}{2}$.

This harmonic Hamiltonian becomes simpler in $\mathbf{k}$ space. We define the Fourier component as $b_{\alpha\mathbf{k}}\equiv\Omega_{\mathbf{n}}^{-1/2}\Sigma_{\mathbf{n}}\exp[-i\mathbf{k}\cdot(\mathbf{n}+\boldsymbol{\delta}_\alpha)]\,b_\alpha(\mathbf{n})$, and also define the vector of the Fourier components by $\boldsymbol{\Psi}_{\mathbf{k}}\equiv{}^t[\,b_{A\mathbf{k}},b_{C\mathbf{k}},b_{D\mathbf{k}},b_{A-\mathbf{k}}^\dagger,b_{C-\mathbf{k}}^\dagger,b_{D-\mathbf{k}}^\dagger\,]$. Using this vector, the Hamiltonian is written in a simple matrix form as usual in the harmonic approximation,

$$
H_{0,HA}/\beta_1=\overline{E}_0+\frac{3}{2}S_\tau^2{\sum_{\mathbf{k}}}'\;\boldsymbol{\Psi}_{\mathbf{k}}^\dagger A_{\mathbf{k}}\boldsymbol{\Psi}_{\mathbf{k}}, \qquad (16)
$$

where $\overline{E}_0\equiv-108S_\tau^2(S_\tau+1)\Omega_{\mathbf{n}}$, and the $\mathbf{k}$ summation is restricted to the half of the Brillouin zone of the simple cubic lattice. The coefficient matrix is

$$
A_{\mathbf{k}}=\begin{bmatrix} B_{\mathbf{k}}+48\mathbb{1} & B_{\mathbf{k}} \\ B_{\mathbf{k}} & B_{\mathbf{k}}+48\mathbb{1}\end{bmatrix}, \qquad (17)
$$

$$
B_k=\begin{bmatrix} 0 & \gamma_{x\mathbf{k}}\gamma_{z\mathbf{k}} & \gamma_{x\mathbf{k}}\gamma_{y\mathbf{k}} \\ \gamma_{z\mathbf{k}}\gamma_{x\mathbf{k}} & 0 & \gamma_{z\mathbf{k}}\gamma_{y\mathbf{k}} \\ \gamma_{y\mathbf{k}}\gamma_{x\mathbf{k}} & \gamma_{y\mathbf{k}}\gamma_{z\mathbf{k}} & 0\end{bmatrix}, \qquad (18)
$$

$$
\gamma_{a\mathbf{k}}\equiv 2\cos\left(\frac{k_a}{2}\right). \qquad (19)
$$

We are ready to diagonalize Hamiltonian (16), and calculate the energy dispersion of excitations in the ordered part. To this end, we need the Bogoliubov transformation of the operators $\{b_{\alpha\mathbf{k}}\}$ and $\{b_{\alpha-\mathbf{k}}^\dagger\}$. Generally, this is not easy when the unit cell contains multiple sites, but this case is exceptionally simple due to the planar nature of the effective model. In the present case, the block-diagonal part in $A_{\mathbf{k}}$ is the same as the block-off-diagonal part aside from the part proportional to the unit matrix. Therefore, these two commute trivially, and we can diagonalize both of them by the same orthogonal matrix $V_{\mathbf{k}}$,

$$
V_{\mathbf{k}}=[\mathbf{v}_{\mathbf{k}}^{(1)},\mathbf{v}_{\mathbf{k}}^{(2)},\mathbf{v}_{\mathbf{k}}^{(3)}],\quad B_{\mathbf{k}}\mathbf{v}_{\mathbf{k}}^{(j)}=\lambda_{j\mathbf{k}}\mathbf{v}_{\mathbf{k}}^{(j)}, \qquad (20)
$$

where the eigenvectors $\mathbf{v}_{\mathbf{k}}^{(j)}$ must be normalized. The eigenvalues are given by

$$
\begin{aligned}
&\lambda_{j\mathbf{k}}=\overline{\lambda}_{\mathbf{k}}\cos(\eta_{\mathbf{k}}+j\phi)\quad(j=1,2,3), \\
&\overline{\lambda}_{\mathbf{k}}\equiv\left[\frac{4}{3}(\gamma_{x\mathbf{k}}^2\gamma_{y\mathbf{k}}^2+\gamma_{y\mathbf{k}}^2\gamma_{z\mathbf{k}}^2+\gamma_{z\mathbf{k}}^2\gamma_{x\mathbf{k}}^2)\right]^{1/2}, \qquad (21) \\
&\eta_{\mathbf{k}}\equiv\frac{1}{3}\cos^{-1}(8\gamma_{x\mathbf{k}}^2\gamma_{y\mathbf{k}}^2\gamma_{z\mathbf{k}}^2/\overline{\lambda}_{\mathbf{k}}^3).
\end{aligned}
$$

Therefore, the Hamiltonian for the wave vector $\mathbf{k}$ is diagonalized in the sublattice space but not yet in the particle-antiparticle space,

$$
\boldsymbol{\Psi}_{\mathbf{k}}^\dagger A_{\mathbf{k}}\boldsymbol{\Psi}_{\mathbf{k}}=\tilde{\Psi}_{\mathbf{k}}^\dagger\begin{bmatrix}\Lambda_k+48\mathbb{1} & \Lambda_{\mathbf{k}} \\ \Lambda_k & \Lambda_{\mathbf{k}}+48\mathbb{1}\end{bmatrix}\tilde{\boldsymbol{\Psi}}_{\mathbf{k}}, \qquad (22)
$$

where

$$
\tilde{\boldsymbol{\Psi}}_{\mathbf{k}}\equiv\begin{bmatrix}{}^tV_{\mathbf{k}} & O \\ O & {}^tV_{\mathbf{k}}\end{bmatrix}\boldsymbol{\Psi}_{\mathbf{k}},\quad \Lambda_{\mathbf{k}}=\mathrm{diag}(\lambda_{1\mathbf{k}},\lambda_{2\mathbf{k}},\lambda_{3\mathbf{k}}). \qquad (23)
$$

Now the three modes are decoupled from each other. The coefficient matrix is two-dimensional in the particle-antiparticle space with the diagonal element $\lambda_{j\mathbf{k}}+48$ and the off-diagonal element $\lambda_{j\mathbf{k}}$. Using the result of usual Bogoliubov transformation, the Hamiltonian H_0 is finally diagonalized,

$$
H_{0,HA}/\beta_1=\overline{E}_0+\frac{3}{2}S_\tau^2{\sum_{\mathbf{k}}}'\sum_{j=1}^{3}\mu_{j\mathbf{k}}\left(\xi_{j\mathbf{k}}^\dagger\xi_{j\mathbf{k}}+\frac{1}{2}\right), \qquad (24)
$$

in terms of boson operators $\boldsymbol{\Phi}_{\mathbf{k}}\equiv{}^t[\,\xi_{1\mathbf{k}},\xi_{2\mathbf{k}},\xi_{3\mathbf{k}},\xi_{1-\mathbf{k}}^\dagger,\xi_{2-\mathbf{k}}^\dagger,\xi_{3-\mathbf{k}}^\dagger]$. The eigenenergy (in units of $\frac{3}{2}S_\tau^2\beta_1$) is given by

$$
\mu_{j\mathbf{k}}\equiv\sqrt{(\lambda_{j\mathbf{k}}+48)^2-\lambda_{j\mathbf{k}}^2}=48\sqrt{1+\frac{1}{24}\lambda_{j\mathbf{k}}}. \qquad (25)
$$

Here the Bogoliubov transformation is defined as

$$
\boldsymbol{\Phi}_{\mathbf{k}}\equiv\begin{bmatrix}X_{\mathbf{k}} & Y_{\mathbf{k}} \\ Y_{\mathbf{k}} & X_{\mathbf{k}}\end{bmatrix}\tilde{\boldsymbol{\Psi}}_{\mathbf{k}}=\begin{bmatrix}X_{\mathbf{k}}\,{}^tV_{\mathbf{k}} & Y_{\mathbf{k}}\,{}^tV_{\mathbf{k}} \\ Y_{\mathbf{k}}\,{}^tV_k & X_{\mathbf{k}}\,{}^tV_{\mathbf{k}}\end{bmatrix}\boldsymbol{\Psi}_{\mathbf{k}}. \qquad (26)
$$

$X_{\mathbf{k}}=\mathrm{diag}(\cosh\varphi_{1\mathbf{k}},\cosh\varphi_{2\mathbf{k}},\cosh\varphi_{3\mathbf{k}})$ and $Y_{\mathbf{k}}=\mathrm{diag}(\sinh\varphi_{1\mathbf{k}},\sinh\varphi_{2\mathbf{k}},\sinh\varphi_{3\mathbf{k}})$, or, explicitly,

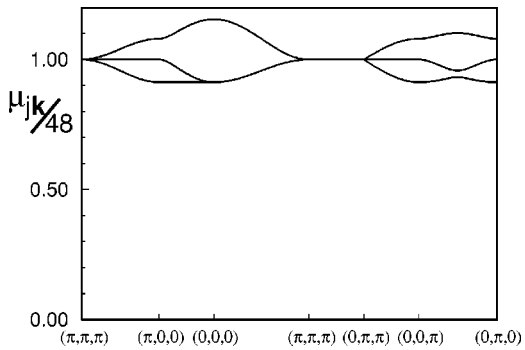

FIG. 5. Normalized dimeron dispersion.

$$\xi_{jk}=\sum_{\alpha=A,C,D}(\mathbf{v}_{\mathbf{k}}^{(j)})_{\alpha}[\cosh\varphi_{j\mathbf{k}}b_{\alpha\mathbf{k}}+\sinh\varphi_{j\mathbf{k}}b_{\alpha-\mathbf{k}}^{\dagger}], \tag{27}$$

$$\xi_{j-\mathbf{k}}^{\dagger}=\sum_{\alpha=A,C,D}(\mathbf{v}_{\mathbf{k}}^{(j)})_{\alpha}[\sinh\varphi_{j\mathbf{k}}b_{\alpha\mathbf{k}}+\cosh\varphi_{j\mathbf{k}}b_{\alpha-\mathbf{k}}^{\dagger}],$$

with

$$\varphi_{j\mathbf{k}}=\frac{1}{2}\tanh^{-1}\frac{\lambda_{j\mathbf{k}}}{\lambda_{j\mathbf{k}}+48}=\frac{1}{4}\log\left(1+\frac{1}{24}\lambda_{j\mathbf{k}}\right). \tag{28}$$

The energy dispersion $\mu_{j\mathbf{k}}$ is shown in Fig. 5. These excitations describe spin-singlet excitations in the part of dimer order, and I will call them ''dimerons'' in this paper.

V. PSEUDOSPIN-DIMERON INTERACTION

The pseudospins on the *B* sublattice are subject to zero molecular field, and they are free in the level of the mean-field approximation. However, they have couplings to dynamic fluctuations in the ordered part. In this section, I derive this coupling in terms of dimeron operators introduced in Sec. IV.

The coupling of pseudospins on the *B* sublattice and those on the other sublattices was already obtained in Eq. (14) in the original τ representation. What we need here is to rewrite the τ operators in the ordered *A*, *C*, and *D* sublattices by dimeron operators ξ and $\xi^{\dagger}$. As shown in Fig. 2, one *B* pseudospin belongs to four pseudospin tetrahedra. Summing up Eq. (14) over these four tetrahedra, the local interaction of the *B*-sublattice pseudospin at position **n** is given as

$$H_1(\mathbf{n})/\beta_1=\frac{1}{2}[Q_+(\mathbf{n})\tau_{B-}(\mathbf{n})+Q_-(\mathbf{n})\tau_{B+}(\mathbf{n})], \tag{29}$$

where $\tau_{B\pm}\equiv\tau_{B1}\pm i\tau_{B2}$ and

$$\begin{aligned}Q_+(\mathbf{n})=e^{-i\phi}[&f_{A-}(\mathbf{n})f_{C+}(\mathbf{n})+f_{A-}(\mathbf{n}+\mathbf{a}_y)f_{C+}(\mathbf{n}-\mathbf{a}_x+\mathbf{a}_y)\\&+f_{A-}(\mathbf{n}+\mathbf{a}_z)f_{C+}(\mathbf{n}-\mathbf{a}_x)+f_{A+}(\mathbf{n}+\mathbf{a}_y+\mathbf{a}_z)f_{C-}\\&\times(\mathbf{n}+\mathbf{a}_y)]+e^{i\phi}[f_{C-}(\mathbf{n})f_{D+}(\mathbf{n})f_{C-}(\mathbf{n}-\mathbf{a}_x)f_{D+}\\&\times(\mathbf{n}-\mathbf{a}_x+\mathbf{a}_z)+f_{C-}(\mathbf{n}+\mathbf{a}_y)f_{D+}(\mathbf{n}+\mathbf{a}_z)\\&+f_{C+}(\mathbf{n}-\mathbf{a}_x+\mathbf{a}_y)f_{D-}(\mathbf{n}-\mathbf{a}_x)]+[f_{D-}(\mathbf{n})f_{A+}(\mathbf{n})\\&+f_{D-}(\mathbf{n}+\mathbf{a}_z)f_{A+}(\mathbf{n}+\mathbf{a}_y+\mathbf{a}_z)+f_{D-}(\mathbf{n}-\mathbf{a}_x)\\&\times f_{A+}(\mathbf{n}+\mathbf{a}_y)+f_{D+}(\mathbf{n}+\mathbf{a}_z-\mathbf{a}_x)f_{A-}(\mathbf{n}+\mathbf{a}_z)],\end{aligned} \tag{30}$$

$$Q_-(\mathbf{n})=[Q_+(\mathbf{n})]^{\dagger},$$

and $f_{\alpha,\pm}(\mathbf{n})\equiv\pm td_{\alpha}(\mathbf{n})+b_{\alpha}(\mathbf{n})^{\dagger}b_{\alpha}(\mathbf{n})$. Here $t=\sqrt{3S_{\tau}/2}$, and $d_{\alpha}=b_{\alpha}+b_{\alpha}^{\dagger}$, as defined above.

As seen in Eqs. (29) and (30), the coupling of free pseudospin to dimerons vanish in the first order of dimeron operators, and starts from the second order. I keep terms of $d_{\alpha}d_{\alpha'}$'s in the local coupling, and rewrite in the **k** presentation. The result reads

$$\begin{aligned}Q_{\pm}^{(2)}(\mathbf{n})=t^2\frac{1}{\Omega_n}\sum_{\mathbf{k},\mathbf{k}'}e^{i(\mathbf{k}+\mathbf{k}')\cdot(\mathbf{n}+\delta_B)}\sum_{j,j'=1}^{3}F_{jj'}^{\pm}(\mathbf{k},\mathbf{k}')\\\times[\xi_{j\mathbf{k}}+\xi_{j-\mathbf{k}}^{\dagger}][\xi_{j'\mathbf{k}'}+\xi_{j'-\mathbf{k}'}^{\dagger}],\end{aligned} \tag{31}$$

where

$$\begin{aligned}F_{jj'}^{\pm}(\mathbf{k},\mathbf{k}')=[&e^{\mp i\phi}f_{AC}(\mathbf{k},\mathbf{k}')(\mathbf{v}_{\mathbf{k}}^{(j)})_A(\mathbf{v}_{\mathbf{k}'}^{(j')})_C\\&+e^{\pm i\phi}f_{CD}(\mathbf{k},\mathbf{k}')(\mathbf{v}_{\mathbf{k}}^{(j)})_C(\mathbf{v}_{\mathbf{k}'}^{(j')})_D+f_{DA}(\mathbf{k},\mathbf{k}')\\&\times(\mathbf{v}_{\mathbf{k}}^{(j)})_D(\mathbf{v}_{\mathbf{k}'}^{(j')})_A]e^{-(\varphi_{j\mathbf{k}}+\varphi_{j'\mathbf{k}'})},\end{aligned} \tag{32}$$

and

$$\begin{aligned}f_{AC}(\mathbf{k},\mathbf{k}')=e^{i(\mathbf{k}+\mathbf{k}')\cdot\boldsymbol{\delta}_B}2\{&\cos[\tfrac{1}{2}(k_z+k_x')]e^{i(k_y+k_y')/2}\\&+\cos[\tfrac{1}{2}(k_z-k_x')]e^{-i(k_y+k_y')/2}\},\\f_{CD}(\mathbf{k},\mathbf{k}')=e^{i(\mathbf{k}+\mathbf{k}')\cdot\boldsymbol{\delta}_B}2\{&\cos[\tfrac{1}{2}(k_y+k_z')]e^{i(k_x+k_x')/2}\\&+\cos[\tfrac{1}{2}(k_y-k_z')]e^{-i(k_x+k_x')/2}\},\\f_{DA}(\mathbf{k},\mathbf{k}')=e^{i(\mathbf{k}+\mathbf{k}')\cdot\boldsymbol{\delta}_B}2\{&\cos[\tfrac{1}{2}(k_x+k_y')]e^{i(k_z+k_z')/2}\\&+\cos[\tfrac{1}{2}(k_x-k_y')]e^{-i(k_z+k_z')/2}\}.\end{aligned} \tag{33}$$

Within this approximation, the coupling of remaining free pseudospins and dimerons in the whole lattice is written as

$$H_1/\beta_1=\frac{1}{2}\sum_{\mathbf{n}}[Q_+^{(2)}(\mathbf{n})\tau_{B-}(\mathbf{n})+Q_-^{(2)}(\mathbf{n})\tau_{B+}(\mathbf{n})]. \tag{34}$$

TABLE II. Normalized coupling constant $\bar{K}_{\alpha\alpha'}=K_{\alpha\alpha'}/\beta_1$. N_r is the number of sites at a distance r.

$r=\|\mathbf{n}\|$	N_r	$\mathbf{n}$	$\bar{K}_{11}(\mathbf{n})$	$\bar{K}_{22}(\mathbf{n})$	$\bar{K}_{12}(\mathbf{n})=\bar{K}_{21}(\mathbf{n})$
1	6	$(\pm1,0,0)$	1.0167×10^{-4}	1.0599×10^{-4}	-0.0374×10^{-4}
		$(0,\pm1,0)$	1.0167×10^{-4}	1.0599×10^{-4}	0.0374×10^{-4}
		$(0,0,\pm1)$	$a_1=1.0815\times10^{-4}$	$b_1=0.9951\times10^{-4}$	0
$\sqrt{2}$	12	$(0,\pm1,\pm1)$	5.5467×10^{-4}	0.5296×10^{-4}	4.3449×10^{-4}
		$(\pm1,0,\pm1)$	5.5467×10^{-4}	0.5296×10^{-4}	-4.3449×10^{-4}
		$(\pm1,\pm1,0)$	$a_{\sqrt{2}}=-1.9789\times10^{-4}$	$b_{\sqrt{2}}=8.0552\times10^{-4}$	0
$\sqrt{3}$	8	$(\pm1,\pm1,\pm1)$	$a_{\sqrt{3}}=1.8738\times10^{-6}$	$b_{\sqrt{3}}=1.8738\times10^{-6}$	0
2	6	$(\pm2,0,0)$	1.6702×10^{-8}	4.7174×10^{-8}	-2.6390×10^{-8}
		$(0,\pm2,0)$	1.6702×10^{-8}	4.7174×10^{-8}	2.6390×10^{-8}
		$(0,0,\pm2)$	$a_2=6.2410\times10^{-8}$	$b_2=0.1466\times10^{-8}$	0

VI. EFFECTIVE PSEUDOSPIN INTERACTION MEDIATED BY DIMERONS

Effective couplings between B-sublattice pseudospins are mediated from this Hamiltonian [Eq. (34)], and I derive it by second-order perturbation. This is analogous to the phonon-mediated electron-electron interaction and also the RKKY interaction between localized spins mediated by their coupling to conduction electrons. In the present case, each fundamental process contains one pseudospin and two dimerons like $\xi^\dagger\xi$ and $\xi^\dagger\xi^\dagger$, not a single dimeron. In the second order of the coupling [Eq. (34)] and at temperature $T=0$, two dimerons are simultaneously created by a local pseudospin flip at a certain position $\mathbf{n}$, and after propagation they are absorbed by a pseudospin at another position n'.

The second-order effective Hamiltonian is defined as $H_B=-\Sigma_{n\neq0}\langle0|H_1|n\rangle\langle n|H_1|0\rangle/(E_n-E_0)$, where the $|n\rangle$'s are dimeron eigenstates and $|0\rangle$ is the dimeron vacuum. As explained above, the relevant intermediate states $|n\rangle$ are dimeron-pair states, $|j\mathbf{k},j'\mathbf{k}'\rangle=\xi^\dagger_{j\mathbf{k}}\xi^\dagger_{j'\mathbf{k}'}|0\rangle$, and so the matrix element becomes

$$\begin{aligned}\langle j\mathbf{k},j'\mathbf{k}'|H_1|0\rangle/(\beta_1 t^2)&=\frac{1}{2}\frac{1}{\Omega_{\mathbf{n}}}\sum_{\mathbf{n}}e^{-i(\mathbf{k}+\mathbf{k}')\cdot(\mathbf{n}+\boldsymbol{\delta}_B)}\{[F^{+}_{jj'}(-\mathbf{k},-\mathbf{k}')\\&+F^{+}_{j'j}(-\mathbf{k}',-\mathbf{k})]\tau_{B-}(\mathbf{n})+[F^{-}_{jj'}(-\mathbf{k},-\mathbf{k}')\\&+F^{-}_{j'j}(-\mathbf{k}',-\mathbf{k})]\tau_{B+}(\mathbf{n})\}.\end{aligned}\tag{35}$$

I take a summation over the intermediate states, and obtain the following effective Hamiltonian:

$$H_B=-\sum_{\mathbf{n},\mathbf{n}'}\sum_{\alpha,\alpha'=1,2}K_{\alpha\alpha'}(\mathbf{n}-\mathbf{n}')\tau_{B\alpha}(\mathbf{n})\tau_{B\alpha'}(\mathbf{n}').\tag{36}$$

Here I drop the constant energy shift due to the self-energy correction, and the coupling constant is given by

$$\begin{bmatrix}K_{11}(\mathbf{n})\\K_{22}(\mathbf{n})\\K_{12}(\mathbf{n})\\K_{21}(\mathbf{n})\end{bmatrix}=\begin{bmatrix}1&1&1&1\\-1&-1&1&1\\i&-i&-i&i\\i&-i&i&-i\end{bmatrix}\begin{bmatrix}D^{--}(\mathbf{n})\\D^{++}(\mathbf{n})\\D^{-+}(\mathbf{n})\\D^{+-}(\mathbf{n})\end{bmatrix},\tag{37}$$

$$\begin{aligned}D^{\nu\nu'}(\mathbf{n})/\beta_1=\frac{3}{16}\frac{1}{\Omega^2_{\mathbf{n}}}\sum_{\mathbf{k}\mathbf{k}'}\sum_{j,j'=1}^{3}\frac{e^{-i(\mathbf{k}+\mathbf{k}')\cdot\mathbf{n}}}{\mu_{j\mathbf{k}}+\mu_{j'\mathbf{k}'}}\\\times[F^{\nu}_{jj'}(\mathbf{k},\mathbf{k}')+F^{\nu}_{j'j}(\mathbf{k}',\mathbf{k})][F^{\nu'}_{jj'}(-\mathbf{k},-\mathbf{k}')\\+F^{\nu'}_{j'j}(-\mathbf{k}',-\mathbf{k})],\quad(\nu,\nu'=\pm).\end{aligned}\tag{38}$$

I numerically calculated the coupling constants using Eqs. (37), (38), (25), and (32). The results for $|\mathbf{n}|\leqslant2$ are shown in Table II. For $|\mathbf{n}|\geqslant\sqrt{2}$, the couplings decay rapidly in space. The value for $|\mathbf{n}|>2$ is order 10^{-8} at most, and I neglect longer-range couplings. Note that, as seen in Table II, the couplings depend also on the direction of $\mathbf{n}$ except for $|\mathbf{n}|=\sqrt{3}$, but they have the same eigenvalues, which are denoted by a_r and b_r $(r=|\mathbf{n}|)$.

VII. ORDER OF PSEUDOSPINS ON THE B SUBLATTICE

In Sec. VI, by considering fluctuations of dimeron-pair processes, I derived the effective interactions between the B-sublattice pseudospins, which remain nonordered in the mean-field level. Now I discuss a possible static order in the B sublattice.

The interactions are not isotropic in the τ_1-τ_2 plane, as shown in Table II, but they have a special kind of symmetry, e.g.,

$$\begin{aligned}K(\pm1,0,0)&=U(-\phi)^{-1}K(0,0,\pm1)U(-\phi),\\K(0,\pm1,0)&=U(\phi)^{-1}K(0,0,\pm1)U(\phi),\\K(0,\pm1,\pm1)&=U(-\phi)^{-1}K(\pm1,\pm1,0)U(-\phi),\\K(\pm1,0,\pm1)&=U(\phi)^{-1}K(\pm1,\pm1,0)U(\phi).\end{aligned}\tag{39}$$

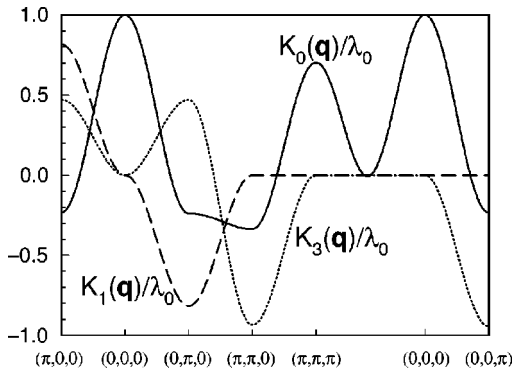

FIG. 6. Wave-vector dependence of the coupling constants K_0, K_3, and K_1, renormalized by the largest eigenvalue, λ_0, defined in Eq. (45).

In order to find the relevant wave vector for symmetry breaking, I calculate the Fourier transform of the couplings, and the result is

$$K(\mathbf{q})=\sum_{\mathbf{n}} K(\mathbf{n})e^{-i\mathbf{q}\cdot\mathbf{n}}=\begin{bmatrix} K_0(\mathbf{q})+K_3(\mathbf{q}) & K_1(\mathbf{q}) \\ K_1(\mathbf{q}) & K_0(\mathbf{q})-K_3(\mathbf{q}) \end{bmatrix}$$
$$=K_0(\mathbf{q})\mathbb{1}+K_3(\mathbf{q})\sigma_3+K_1(\mathbf{q})\sigma_1, \tag{40}$$

with σ_1 and σ_3 being the Pauli matrices. The parameters here are defined as

$$3K_0(\mathbf{q})=s_{1+}(\cos q_x+\cos q_y+\cos q_z)$$
$$+s_{\sqrt{2}+}(\cos q_x\cos q_y$$
$$+\cos q_y\cos q_z+\cos q_z\cos q_x)$$
$$+s_{\sqrt{3}+}3\cos q_x\cos q_y\cos q_z$$
$$+s_{2+}(\cos 2q_x+\cos 2q_y+\cos 2q_z), \tag{41}$$

$$3K_3(\mathbf{q})=s_{1-}[\cos q_z-\tfrac{1}{2}(\cos q_x+\cos q_y)]$$
$$+s_{\sqrt{2}-}[\cos q_x\cos q_y-\tfrac{1}{2}(\cos q_y\cos q_z$$
$$+\cos q_z\cos q_x)]+s_{2-}[\cos 2q_z-\tfrac{1}{2}(\cos 2q_x$$
$$+\cos 2q_y)], \tag{42}$$

$$3K_1(\mathbf{q})=s_{1-}\frac{\sqrt{3}}{2}(\cos q_y-\cos q_x)$$
$$+s_{\sqrt{2}-}\frac{\sqrt{3}}{2}(\cos q_z\cos q_x-\cos q_y\cos q_z)$$
$$+s_{2-}\frac{\sqrt{3}}{2}(\cos 2q_y-\cos 2q_x), \tag{43}$$

with $s_{r\pm}\equiv N_r(a_r\pm b_r)/2$ defined by the values listed in Table II. Figure 6 shows these parameters along symmetric axes in the Brillouin zone.

In the classical limit ($S_\tau\to\infty$), the long-range order is determined from the largest eigenvalue of the coupling constant $K(\mathbf{q})$. The eigenvalues are

$$\lambda_\pm(\mathbf{q})=K_0(\mathbf{q})\pm\sqrt{K_3(\mathbf{q})^2+K_1(\mathbf{q})^2}, \tag{44}$$

and they take a maximum value at $\mathbf{q}=0$,

$$\lambda_0=\lambda_+(\mathbf{0})=\sum_r s_{r+}=K_0(\mathbf{0}), \tag{45}$$

and this value is $4.2839\times10^{-3}\beta_1$ calculated from the data in Table II. Around $\mathbf{q}\sim\mathbf{0}$, the eigenvalues are expanded as

$$\lambda_\pm(\mathbf{q})\sim\lambda_0-c_2\mathbf{q}^2\pm c_4\sqrt{\tfrac{3}{2}(q_x^4+q_y^4+q_z^4)-\tfrac{1}{2}(\mathbf{q}^2)^2}, \tag{46}$$

$$c_2=\tfrac{1}{6}\sum_r r^2 s_{r+},\quad c_4=\tfrac{1}{6}(s_{1-}-s_{\sqrt{2}-}+4s_{2-}), \tag{47}$$

and the value of the parameters is $c_2=1.3267\times10^{-3}\beta_1$ and $c_4=1.0078\times10^{-3}\beta_1$. Since the eigenvalue is maximized at the wave vector $\mathbf{q}=\mathbf{0}$, a uniform order is realized.

Next I discuss the direction of this ordered moment in the B sublattice. To this end, we need to look at the anisotropy of the coupling constant $K(\mathbf{q})$. First of all, recall that the pseudospins are interacting only in the τ_1-τ_2 plane, but not in the τ_3 direction. Second, at $\mathbf{q}=\mathbf{0}$, the coupling is isotropic in the τ_1-τ_2 plane, $K(\mathbf{0})=\lambda_0\mathbb{1}$. Therefore, in the level of the mean-field approximation (equivalent to the classical limit), the spontaneous moment is aligned in any direction in the τ_1-τ_2 plane. However, the coupling constant in the effective model [Eq. (36)] is not isotropic for general $\mathbf{n}$, and this is more clearly shown as the presence of anisotropic parts, $K_3(\mathbf{q})$ and $K_1(\mathbf{q})$, in the Fourier component. Therefore, when fluctuations around the mean-field ground state are concerned, we expect that some special directions will be favored. I discuss this problem in Sec. VIII.

I examine the quantum fluctuations around the mean-field ground state of a B-sublattice pseudospin. As before, I use the Holstein-Primakoff bosonization and the harmonic approximation for fluctuations. Let us parametrize the mean-field ground state by the direction of the ordered moment, $\langle\tau_B(\mathbf{n})\rangle=(\cos\theta,\sin\theta,0)$. I treat this angle θ as a variational parameter, and will calculate the quantum zero-point energy as a function of this angle, $\Delta E_B(\theta)$, to check the stability of this state. The calculations are all done in parallel to those for the dimeron spectrum in Sec. IV. Since the unit cell now contains only a single B-sublattice site, the calculations are straightforward. The result of linearized Hamiltonian is

$$H_{B,HA}=-4\Omega_{\mathbf{n}}S_\tau(S_\tau+1)\lambda_0$$
$$+2S_\tau{\sum_{\mathbf{k}}}'\,\psi_{\mathbf{k}}^\dagger\begin{bmatrix} 4\lambda_0-2\tilde{K}_{22}(\mathbf{k}) & -2\tilde{K}_{22}(\mathbf{k}) \\ -2\tilde{K}_{22}(\mathbf{k}) & 4\lambda_0-2\tilde{K}_{22}(\mathbf{k}) \end{bmatrix}\psi_{\mathbf{k}}, \tag{48}$$

where the $\mathbf{k}$ summation is taken over a half of the Brillouin zone of the cubic lattice, $\psi_{\mathbf{k}}^\dagger=[b_{B\mathbf{k}}^\dagger,b_{B-\mathbf{k}}]$ are the Holstein-Primakoff boson operators, and

$$\tilde{K}_{22}(\mathbf{k})=K_0(\mathbf{k})-K_3(\mathbf{k})\cos 2\theta-K_1(\mathbf{k})\sin 2\theta, \tag{49}$$

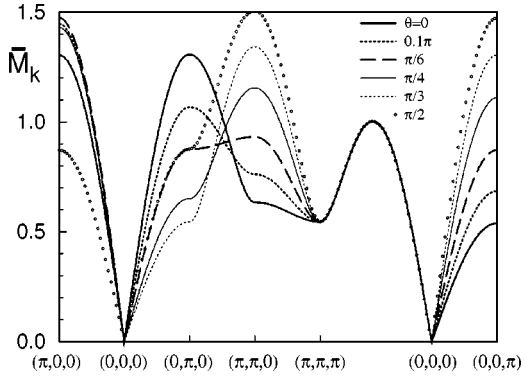

FIG. 7. Wave-vector dependence of the renormalized eigenenergy $\bar{M}_{\mathbf{k}}$, for several θ's.

depends on the variational angle parameter θ. Applying the Bogoliubov transformation $\xi_{B\mathbf{k}}=b_{B\mathbf{k}}\cosh\varphi_{B\mathbf{k}}-b^{\dagger}_{B-\mathbf{k}}\sinh\varphi_{B\mathbf{k}}$, with $\varphi_{B\mathbf{k}}=1/2\coth^{-1}[2\lambda_0/\tilde{K}_{22}(\mathbf{k})-1]$, we finally obtain the diagonalized Hamiltonian

$$H_{B,HA}=\left(1+\frac{1}{S_\tau}\right)E_{B,0}+8S_\tau\lambda_0\sum_{\mathbf{k}}\bar{M}_{\mathbf{k}}\left(\xi^{\dagger}_{B\mathbf{k}}\xi_{B\mathbf{k}}+\frac{1}{2}\right), \tag{50}$$

with $E_{B,0}=-4\Omega_{\mathbf{n}}S_\tau^2\lambda_0$ is the mean-field ground-state energy of the B-sublattice order, and

$$\bar{M}_k=\left(1-\frac{\tilde{K}_{22}(\mathbf{k})}{\lambda_0}\right)^{1/2}, \tag{51}$$

is the eigenenergy of excitations in units of $8S_\tau\lambda_0$. The dispersion of $\bar{M}_k$ is plotted in Fig. 7 for typical values of θ. When $\mathbf{k}\to\mathbf{0}$, the anisotropic parts of the coupling constant, K_3 and K_1, becomes zero as seen from Eqs. (42) and (43), and therefore, $\tilde{K}_{22}(\mathbf{k})\to K_0(\mathbf{0})=\lambda_0$. Therefore, on approaching the $\mathbf{k}=\mathbf{0}$ point, the excitation energy $8S_\tau\lambda_0\bar{M}_{\mathbf{k}}$ always goes to zero ''linearly,'' but with an anisotropic velocity:

$$\bar{M}_{\mathbf{k}}\sim\sqrt{\frac{c_2}{6\lambda_0}(c_xk_x^2+c_yk_y^2+c_zk_z^2)}, \tag{52}$$

$$\left.\begin{matrix}c_x\\c_y\\c_z\end{matrix}\right\}=1-\frac{c_4}{c_2}\times\left\{\begin{matrix}\cos(2\theta+\phi)\\\cos(2\theta-\phi)\\\cos(2\theta)\end{matrix}\right. . \tag{53}$$

The ratio $c_4/c_2=0.7597$ is smaller than unity, and therefore these c's are positive for any θ.

The ground-state energy of the Hamiltonian is obviously

$$E_{B,HA}(\theta)=\left(1+\frac{1}{S_\tau}\right)E_{B,0}+4S_\tau\lambda_0\sum_{\mathbf{k}}\bar{M}_{\mathbf{k}}, \tag{54}$$

and this depends on the θ parameter, inherited from the θ dependence of $\tilde{K}_{22}$. The correction due to quantum fluctuations, ΔE_B, has a relative factor $1/S_\tau$ compared to the mean-field value, and I parametrize it by a function of order S_τ^0, and R, as

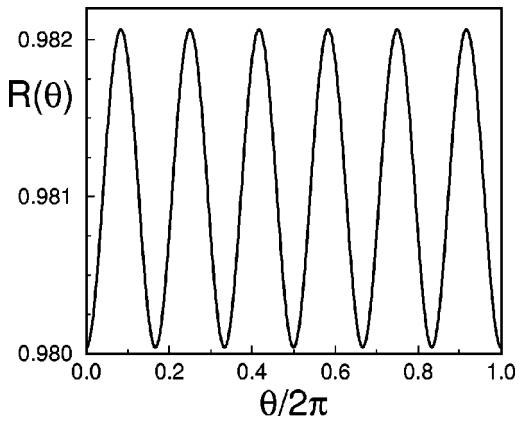

FIG. 8. Dependence of the zero-point energy on the direction of the ordered moment.

$$\Delta E_B(\theta)=E_{B,HA}-E_{B,0}=\frac{1}{S_\tau}|E_{B,0}|[-1+R(\theta)]. \tag{55}$$

The part of -1 here corresponds to the contribution of the first term on the right-hand sides Eq. (54). We can determine the stable direction of the spontaneous order by the calculation of $R(\theta)$. This is explicitly expressed as

$$\begin{aligned}R(\theta)&=\frac{1}{\Omega_{\mathbf{n}}}\sum_{\mathbf{k}}\bar{M}_{\mathbf{k}}=\frac{1}{\Omega_{\mathbf{n}}}\sum_{\mathbf{k}}\left(1-\frac{\tilde{K}_{22}(\mathbf{k})}{\lambda_0}\right)^{1/2}\\&=\frac{1}{\Omega_{\mathbf{n}}}\sum_{\mathbf{k}}\left[1-\frac{1}{\lambda_0}[K_0(\mathbf{k})-K_3(\mathbf{k})\cos 2\theta\right.\\&\qquad\left.-K_1(\mathbf{k})\sin 2\theta]\right]^{1/2},\end{aligned} \tag{56}$$

and the value is always less than unity. This implies that $-1+R(\theta)<0$ for all θ, meaning that the quantum fluctuations always lower the ground-state energy, as expected.

Figure 8 shows the result of numerical calculation for $R(\theta)$. Although the θ dependence is very small, I have checked that it is not a numerical error but is intrinsic. Upon the numerical summation for Eq. (56), I systematically increased the number of $\mathbf{k}$ points up to 512^3, and confirmed a fairly well convergence. This result is well approximated by a simple harmonic function,

$$R(\theta)\approx 0.98106-0.00101\cos 6\theta, \tag{57}$$

and have the minimum value at $\theta=0$, $\pm\phi/2$, $\pm\phi$, and π. The amplitude of other harmonics is very small, $\sim 10^{-5}$ at most. A similar θ dependence is reproduced by replacing $\bar{M}_{\mathbf{k}}$ by its continuum limit [Eq. (52)], and therefore the anisotropy may be due to fluctuations with long wavelength.

As discussed in Sec. III, the points of $\theta=0$ and $\pm\phi$ correspond to the order of dimer pairs in the B-sublattice tetrahedra, while the other points $\theta=\pm\phi/2$ and π correspond to tetramer orders. Therefore, we come to the conclusion that the B-sublattice tetrahedra will ultimately reveal a uniform long-range order of either dimers or tetramers.

VIII. CONCLUSIONS AND DISCUSSIONS

In this paper, I have investigated the ground state of a quantum Heisenberg antiferrmagnet on the pyrochlore lattice. Here I summarize and reinterpret the results of this paper in the original spin picture instead of the pseudospin representation used in the previous sections.

My approach is based on the basic assumption that the spin-triplet sector has a finite-energy gap from the singlet ground state, and that the low-energy dynamics can be well described in terms of local singlet basis. I employed the effective Hamiltonian which was obtained for the singlet sector in Ref. 9, and determined its ground state beyond the mean-field approximation. I accomplished this by taking account of the effects of quantum fluctuations in four stages. I also clarified the nature of various elementary excitations in this system, and calculated their energy scales.

An important parameter characterizing quantum fluctuations is determined by the number of local singlet states $(2S_\tau+1)$ and the number of local processes $(N_{\mathrm{proc.}})$: it is $1/(S_\tau \times N_{\mathrm{proc.}})$, as expected from the analogy to the spin-wave theory. Although S_τ is 1/2 in the present case, $N_{\mathrm{proc.}}$ is large because of large connectivity in the effective models: 12 elementary triangle faces for the fcc lattice and six neighbor sites for the simple cubic lattice. Therefore, this parameter becomes small, and this may justify the harmonic approximation used in the present work to treat quantum fluctuations.

The mean-field picture of the effective model in the previous studies is the coexistence of a long-range order of spin-singlet dimers and a non-ordered spin-singlet part. The non-ordered part has large local fluctuations of both the spin chirality and dimer pattern, and no long-range order is stabilized. In the first stage of this paper, I determined elementary excitations in the dimerized part. They are spin-singlet excitations, and mainly correspond to the deformation of dimer configuration; I called them *dimerons*. In the second stage, I calculated the coupling of the nonordered spin-singlet part and the dimeron excitations, and I found that the fundamental processes involve the creation and annihilation of a dimeron pair. In the third stage, I derived the effective interaction between two nonordered singlets mediated from a coupling to dimeron pairs. It is a model in which fluctuations of the dimer channel are coupled to each other between two nonordered positions, and the favored local pattern depends on the configuration of the dimer pattern in the surrounding ordered part. On the other hand, there is no coupling in the chirality channel within the present approach. In the last stage, I determined the ground state of this effective model, and discussed the final form of spin order in the spin-singlet sector. I found that the uniform spatial arrangement has the lowest energy, and that the energy gain is identical to any quantum mixture of local dimer and tetramer states within the mean-field level. However, it turns out that the quantum fluctuations favor one of the three pure dimer states or the three pure tetramer states. All the pure dimer states are equivalent to each other, and this is also the case for the tetramer order.

Figure 9 shows the finally determined ground-state spin configuration of the whole system. It is shown for the cubic unit cell of the pyrochlore lattice. One is for the case of all dimers, and the other is for the case of a mixture of six dimers and one tetramer.

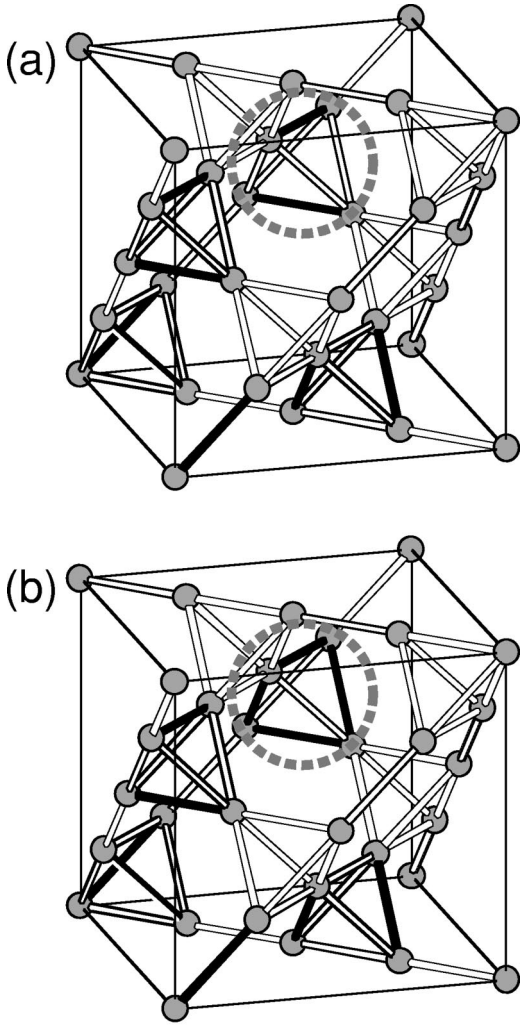

FIG. 9. Spin configuration in the ground state with singlet order. The hardly ordered part (*B*-sublattice in Fig. 1) is indicated by dotted circle. (a) All-dimer pattern. (b) Mixture of dimers and tetramer. Dimers and tetramers are shown in black.

I now summarize the various types of elementary excitations and their energy scale. First of all, the original Heisenberg spin model is believed to have a finite spin gap, i.e., a singlet-triplet energy gap; the spin-triplet excitations are quantum (para) magnons. A spin-triplet sector was already traced out when my starting Hamiltonian in the singlet sector was derived, and we need to go back to the original Heisenberg model to determine the value of the spin gap and the magnon dispersion, which I did not study in the present paper. The excitations studied in this paper are all of spin singlet type, and they may be understood in the following way. The second type of excitations corresponds to the deformation of the dimer pattern in the easily ordered part, and they are called ''dimerons'' in this paper. They have a dispersion $\beta_1 \frac{3}{2} S_\tau^2 \mu_{j\mathbf{k}}$, shown in Fig. 5, and their energy gap is finite. The large energy gap means that the dimer order in the easily

ordered part is quite stable, and fluctuations of the dimer pattern in this part are small in amplitude and short ranged.

The third type of excitations corresponds to collective deformations of the dimer or tetramer pattern in the hardly ordered part. In this sense, they are also a kind of dimeron excitation, but the energy scale and the dispersion are different from those in the easily ordered part. They have the dispersion $8S_\tau\lambda_0\overline{M}_{\mathbf{k}}$ shown in Fig. 7, and the energy gap is zero. Since $\lambda_0/\beta_1<10^{-2}$ in addition to a further reduction factor, the energies of these excitations are well below the gap of the dimeron dispersion in the easily ordered part. The bandwidth of these excitations is very small, because the dimers and tetramers in the hardly ordered part interact only through the coupling to dimeron excitations in the easily ordered part, which decay rapidly in space. The zero gap of these excitations is reminiscent of the Goldstone mode for the systems with continuous symmetry. However, our model does not hold the rigorous rotation symmetry in the space of dimer and tetramer patterns. Therefore, there may appear a finite energy gap, when the nonharmonicity of quantum fluctuations is taken into account. However, even if this is the case, the size of the generated gap will be very small.

An important open problem is the interaction between triplet magnons and singlet dimerons. This interaction will play a crucial role when the system approaches a magnetic instability.

Finally, I emphasize the presence of a hierarchical structure of energy scales corresponding to different types of excitations. This point may be one of the main features of geometrically frustrated quantum magnets. When geometrical frustrations are strong, the construction of the ultimate ground state needs complicated processes, and this will take place successively on different length scales. That is, in one stage, a part of degrees of freedom are to be arranged in a clever way to gain energy, but other parts remain frustrated until the next stage. This process repeats with the reduction of the energy scale, until all the degrees of freedom are used up. A hierarchical structure of the relevant energy scales is thus expected, corresponding to multiple stages in the successive stabilization processes. Therefore, this feature is expected to be common in many geometrical frustrated systems.

ACKNOWLEDGMENTS

This work was supported by a Grant-in-Aid from the Ministry of Education, Science, Sports and Culture of Japan. A part of the numerical calculations were performed on supercomputers at the Institute for Solid State Physics, University of Tokyo.

[1] See a recent review by A. P. Ramirez, in *Handbook of Magnetic Materials*, edited by K. H. J. Buschow (North-Holland, Amsterdam, 2001), Vol. 13; also see papers cited therein.
[2] R. Liebmann, *Statistical Mechanics of Periodic Frustrated Ising Systems* (Springer, Berlin, 1986).
[3] J. Villain, Z. Phys. B: Condens. Matter **33**, 31 (1979).
[4] P. W. Anderson, Phys. Rev. **102**, 1008 (1956).
[5] A. B. Harris, J. Berlinsky, and C. Bruder, J. Appl. Phys. **69**, 5200 (1991).
[6] B. Canals and C. Lacroix, Phys. Rev. Lett. **80**, 2933 (1998).
[7] A. Koga and N. Kawakami, Phys. Rev. B **63**, 144432 (2001).
[8] Y. Yamashita and K. Ueda, Phys. Rev. Lett. **85**, 4960 (2000).
[9] H. Tsunetsugu, J. Phys. Soc. Jpn. **70**, 640 (2001).
[10] M. Troyer, H. Tsunetsugu, and D. Würtz, Phys. Rev. B **50**, 13 515 (1994).
[11] F. Mila, Phys. Rev. Lett. **81**, 2356 (1998).
[12] For example, T. Inui, Y. Tanabe, and Y. Onodera, *Group Theory and Its Applications in Physics* (Springer, Heidelberg, 1996).
[13] See advanced textbooks on magnetism, for example, A. Auerbach, *Interacting Electrons and Quantum Magnetism* (Springer, Berlin, 1994).